THE JOURNAL OF PHYSICAL CHEMISTRY B

Article

pubs.acs.org/JPCB

Binding Interaction and Rotational-Relaxation Dynamics of a Cancer Cell Photosensitizer with Various Micellar Assemblies

Bijan Kumar Paul,[†,§] Debarati Ray,[†] and Nikhil Guchhait*

Department of Chemistry, University of Calcutta, 92 A. P. C. Road, Calcutta-700009, India

ABSTRACT: The present work demonstrates the photophysical characterization of the interaction of a promising cancer cell photosensitizer, harmane (HM), with biomimetic micellar nanocavities having varying surface charge characteristics. The polarity-sensitive prototropic transformation of HM is remarkably modified upon interaction with the macromolecular assemblies of micellar systems and is manifested through significant modulations on the absorption and emission profiles of HM. The ground- and excited-states prototropic equilibria of HM are found to be differentially modulated in various micellar assemblies. Out of various possibilities to assess the drug (HM)−micelle interaction mechanism, the postulate of varying extent of drug penetration into micellar units depending on the compactness of their headgroup arrangements is found to suitably rationalize and correlate different experimental findings, including the differences in binding constant (K) and free energy change (ΔG) of the interaction process. The micropolarity measurement has been exploited to evaluate the probable binding location of the drug which reveals that the cationic drug molecule does not penetrate deep into the micellar core region and the results are further substantiated from fluorescence quenching experiments. The work also pays proper attention to delineate the modulation in dynamical behaviors of the drug following interaction with the micellar systems. Wavelength-sensitive fluorescence parameters reveal the slower rate of solvent-relaxation around the excited probe within the micelle-encapsulated microheterogeneous environments. The enhancement of fluorescence anisotropy and rotational relaxation time of the drug in micellar environments from that in pure aqueous buffer suggests entrapment of the drug in motionally constrained regions introduced by the micelles.

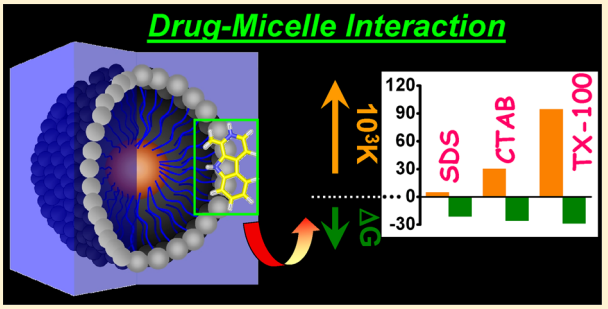

1. INTRODUCTION

Recently, enormous attention has been given to the investigation of structure and properties of chemical entities entrapped in molecular assemblies like cyclodextrins, micelles, reverse micelles, microemulsions, vesicles, etc. compared to that in pure homogeneous media.[1−11] This is because of the promising prospects of organized assemblies on biological, photochemical, and photophysical processes. Micelles are one of such organized assemblies that has formed the nucleus of many-faceted research activities over the past few years.[6,10,11] Micelles are highly cooperative, thermodynamically stable, dynamic nanostructures formed out of amphiphilic surfactant molecules above a critical concentration (precisely a narrow concentration range) known as the critical micellar concentration (CMC). The interactive nature of innumerous fluorophores in micellar systems has been quite extensively addressed in the literature mainly with a view to the ability of such dynamic nanostructures to mimic biological membranes in a much simpler model.[11,12] Such studies have significance in fundamental research also because of their ability to furnish valuable information about the underlying noncovalent intermolecular forces.[1] In principle, the instrumental role of noncovalent intermolecular forces (particularly the hydrophobic effect) responsible for micelle formation is common to other related assemblies such as reverse micelles, liposomes, bilayers and biological membranes.[11,12] Apart from the inherent compositional and functional complexities associated with true biological membranes that have promoted research with relatively simpler micellar model systems, some additional technical edges are often obtained with micelles, e.g., they are optically transparent, spectroscopically silent, and relatively scatter free. Furthermore, the promising prospects in future applications like targeted drug delivery,[3] nanometer sized electronic devices,[4] development of energy storage devices,[5] etc. have enormously contributed to the growing interest in research with various micellar systems.

Characterization of drug molecules owes paramount significance when it is related with a detrimental disease because the number of available drugs in the literature for the treatment of such diseases is sparse. The naturally occurring alkaloid β-carbolines have captured much attention over the past few years given the wide range of biological properties, which include their functioning as potential monoamine-oxidase (MAO) enzyme inhibitors and their interaction with a considerable number of neurotransmitters and neuro-modulators of the central nervous system (CNS).[13−15] Additionally, the novel biological application of β-carbolines in the form of photosensitizer to fungi, viruses, bacteria, etc. has

Received: May 3, 2012
Revised: June 13, 2012
Published: July 11, 2012

dx.doi.org/10.1021/jp304280m | J. Phys. Chem. B 2012, 116, 9704−9717

been central to an immensely important topic of research in medical science: photodynamic therapy (PDT).[16−18] β-Carbolines are reported to be effective in producing singlet oxygen which is detrimental to cancerous/malignant cells.[18,19] Such a wide range of biological activities surrounding β-carbolines has played a pivotal role in forming the nucleus of research to investigate the interaction of these derivatives with biological/biomimicking receptors.

The field of interaction of β-carbolines with biological receptors still awaits meticulous exploration. Additionally, the studied β-carboline derivative HM has remained comparatively underutilized in these perspectives.[20] Trapping of such biologically potent drugs in different biomimetic environments becomes attractive because of their ability to achieve special chemical efficiency as a result of organization in the reaction media. Successful application of micelles in loading and targeted delivery of drugs and biodetoxofication of drugs (a process in which empty micelles can act as sinks to scavenge the drug in blood circulation and prevents its toxic effects) demands meticulous characterization of the interaction of the drug with the concerned micellar system. The present program is focused on exploring the interaction of the prospective drug molecule harmane (HM) with micellar assemblies having varying surface charges, e.g., anionic micelle sodium dodecyl sulfate (SDS), cationic micelle cetyltrimethyl ammonium bromide (CTAB), and neutral micelle *p-tert*-octylphenoxy polyoxyethanol, i.e., Triton X-100 (TX-100) (Scheme 1).

Scheme 1. (a) Simplified Paradigm Showing the Cation ⇌ Neutral Prototropic Equilibrium in HM and (b) Chemical Structures of the Surfactant Molecules Studied

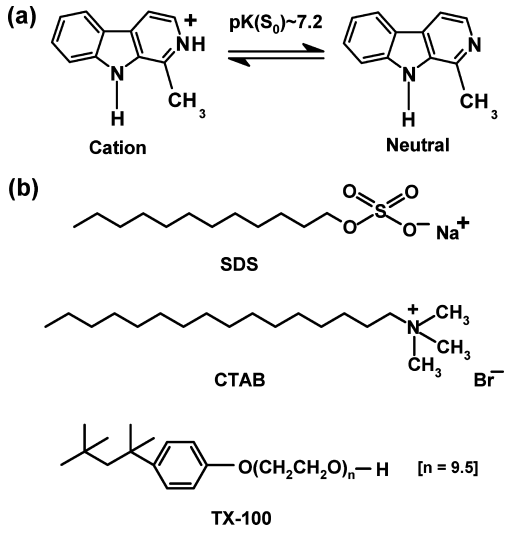

Owing to the amphiphilic character of surfactant molecules, they can modify a reaction to a considerable extent if there is a charge separation during the process.[21] The pyridine ring in HM is electron deficient and the indole ring is electron excess resulting in two functional sites for acid−base chemistry which is sensitive to the variation of medium polarity.[20,22,23] The polarity-dependent prototropic transformation of HM (Scheme 1) is found to be differentially modulated within the micellar assemblies having varying surface charges and is reflected on the absorption and emission spectral profiles. The results of the present investigation reveal the conjugate effect of polarity and confinement on the photophysics and motional restriction of the drug within the micellar assemblies. The effect of micellar entrapment on the dynamical behavior of the drug is also investigated in this context. The work also pays attention to the modulations in rotational-relaxation dynamics of the drug within micellar nanocavities.

Usually biologically active materials for therapeutic activities are selected with a view to the pharmacokinetic and pharmacodynamic behavior of the exogeneous materials within the body, which yield a rational understanding of the ADME (absorption, distribution, metabolism, and excretion) characteristics of the drugs. The appropriate selection of the drug delivery vehicle naturally constructs an indispensable element of research along this direction. Despite the mushrooming efforts inclined to this direction, a large part of the research in the sector still dwells at the stage of prospect and proposition. In the late 1960s, micelles captured considerable attention as prospective drug delivery vehicles owing to their controllable properties and benign pharmacoligal behavior.[24,25] Micelles can offer a score of advantages as drug carriers. First, micelles can encapsulate sparingly soluble pharmaceuticals and deliver them to the site of action at concentrations which can even exceed their intrinsic water solubility, hence enhancing their bioavailability.[26,27] It has been particularly emphasized in this context[26] that entrapment of bioactive materials in micellar assemblies is principally governed by noncovalent interactions which in turn evinces no alteration of the chemical properties of the drugs. This aspect in materializing micelles as prospective drug carriers has received much attention in complicated fields, e.g., photodynamic therapy and chemotherapy particularly given the high degree of insolubility in water of a large part of newly discovered drugs, as has been argued in recent reviews.[27−29] Further, with micelle-encapsulated drugs, the probability of undesirable side effects arising out of contact of the drug with inactivating species, such as enzymes present in biological fluids, is minimized, as compared with those of free drug.[27−29] The small nanoscopic dimension and narrow size distribution of micellar units provides a marked edge in terms of retarding the rate of body clearance through renal filtration.[26,27] Recently, chemical modifications of the surfactant molecules with intentions to modulate the micellar properties are also being tested for the use of micelles as delivery vehicles of photosensitizers in PDT.[29] However, in order to achieve the desired degree of implementation in this research arena, investigation of the properties of photosensitizers in relatively simple micellar systems might provide a simple basis before moving onto the complex systems. This can be fruitful in assessing not only the behavior of the photosensitizers in drug delivery vehicles but also in complementing required modifications for future applications. Furthermore, the interaction of drugs with micellar assemblies also is significant in view of the ability of micellar systems to mimic complex biological membranes in a much simpler model.[11,12]

2. EXPERIMENTAL SECTION

2.1. Materials. HM procured from Sigma Chemical Co., USA was used as received. The purity of the compound was tested on a TLC plate before use. The surfactants sodium dodecyl sulfate (SDS), cetyltrimethyl ammonium bromide (CTAB), and TX-100 were procured from Sigma Chemical Co. and used without further purification. No contribution of the surfactant solutions on either absorption or fluorescence in the studied wavelength region was affirmed prior to their use in the present study. Tris buffer and hydrochloric acid (HCl) from E-

dx.doi.org/10.1021/jp304280m | J. Phys. Chem. B 2012, 116, 9704−9717

Merck were used to prepare the Tris-HCl buffer (pH 7.4) in deionized water from Milli-Q water purification system (Millipore). The solvent 1,4-dioxane was of UV Spectroscopy grade (Spectrochem, India).

Copper(II) perchlorate ($Cu(ClO_4)_2 \cdot 6H_2O$) and potassium bromide (KBr) for fluorescence quenching studies were procured from Sigma-Aldrich, USA and used as received.

2.2. Instrumentation and Methods. *Steady-State Spectral Measurements.* The absorption and emission spectra were acquired on Hitachi UV−vis U-3501 spectrophotometer and Perkin-Elmer LS55 fluorimeter, respectively. The concentration of HM was maintained at ∼2.0 μM (in order to eliminate the possibilities of aggregation and reabsorption) and pH at 7.40 throughout the study.

Steady-State Fluorescence Anisotropy. Steady-state fluorescence anisotropy was measured on Perkin-Elmer LS55 fluorimeter. The steady-state anisotropy (r) is defined as[30]

$$r = \frac{(I_{VV} - GI_{VH})}{(I_{VV} + 2GI_{VH})} \quad (1)$$

$$G = \frac{I_{HV}}{I_{HH}} \quad (2)$$

where I_{VV} and I_{VH} are the emission intensities when the excitation polarizer is vertically oriented and the emission polarizer is oriented vertically and horizontally, respectively. G is the correction factor.

Time-Resolved Measurements. The time-resolved fluorescence decays were acquired on FluoroCube-01-NL spectrometer based on the time-correlated single photon counting (TCSPC) technique using a nanoLED at 340 nm and a Laser diode at 375 nm as the light sources to trigger the fluorescence of neutral and cationic species of the drug HM, respectively, and the signals were collected at the magic angle of 54.7° to eliminate the contribution from anisotropy decay.[30] The decays were deconvoluted and analyzed on DAS-6 decay analysis software.[20,22,23,30] Mean (average) fluorescence lifetime ($\langle\tau_{i0}\rangle$) was calculated from the equation[30]

$$\langle\tau_{i0}\rangle = \frac{\sum_i \alpha_i \tau_i^2}{\sum_i \alpha_i \tau_i} \quad (3)$$

in which α_i represents the relative amplitude of the ith component of decay having the characteristic decay time constant τ_i, such that $\sum_i \alpha_i = 1$. The quality of the fits was judged from χ^2 criterion and visual inspection of the residuals of the fitted functions to the actual data.

For time-resolved fluorescence anisotropy decay measurements, the polarized fluorescence decays for the parallel $[I_{\parallel}(t)]$ and perpendicular $[I_{\perp}(t)]$ emission polarizations with respect to the vertical excitation polarization were first collected at the emission maxima of the probe. The anisotropy decay function $r(t)$ was constructed from these $I_{\parallel}(t)$ and $I_{\perp}(t)$ decays using the following equation:[30]

$$r(t) = \frac{I_{\parallel}(t) - GI_{\perp}(t)}{I_{\parallel}(t) + 2GI_{\perp}(t)} \quad (4)$$

G is the correction factor for the detector sensitivity to the polarization detection of the emission.

Dynamic Light Scattering. Dynamic light scattering (DLS) measurements were carried out on a Malvern Nano-ZS instrument employing a 4 mW He−Ne LASER (λ = 632.8 nm) and equipped with a thermostatted sample chamber. The sample was poured into a DTS0112 low volume disposal sizing cuvette of 1.5 mL (path-length 1 cm). The operating procedure was programmed by the Malvern instrument software in a fashion that there was an average of 25 runs, each run being averaged for 15 s, and then a particular hydrodynamic diameter and size distribution was extracted using the DTS software.

All experiments were performed at an ambient temperature of 300.0 K unless otherwise specified.

Deconvolution of Spectra. The experimentally obtained spectra were analyzed by deconvolution into overlapping Gaussian curves using the Marquardt−Levenberg algorithm as implemented in MS Origin 7 to obtain the minimum number of reproducible spectral components using the adjustable parameters of the center, width, and amplitude of each Gaussian curve.[31] Multiple attempts to fit the data with different starting parameters can generally provide a survey of the extent of statistically equivalent parameter sets.[31] Comparing several deconvolutions of an overall spectrum, a "good" fit is then judged by several criteria including a minimum in the goodness-of-fit parameter χ^2 (the weighted sum of the squares of the deviations)[31] and a maximum value for the square of the multiple correlation coefficient, r^2.[31] From these statistically acceptable fits, a "good" fit is further judged by the reproducibility in the values for the centers of the Gaussian curves. A final, albeit subjective, criterion was to examine the fits for physically plausible results.

3. RESULTS AND DISCUSSION

3.1. Steady-State Absorption and Emission Studies. The absorption profile of HM is characterized by two distinct broad bands at $\lambda_{abs} \approx$ 348 nm and 370 nm in aqueous buffer (Figure 1a). The photophysical properties of various β-carboline derivatives have long been seen as an intriguing topic of research and have been addressed quite extensively in the literature.[20,22,23,32,33] In analogy to literature re-

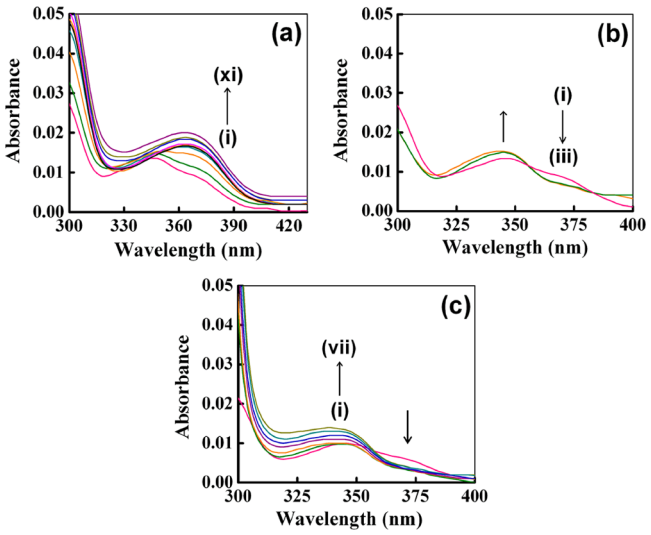

Figure 1. Representative absorption spectral profile of HM in aqueous buffer medium in the presence of increasing concentrations of (a) SDS, (b) CTAB, and (c) TX-100. In panel (a) curves (i) → (ix) correspond to [SDS] = 0.0, 0.5, 1.0, 1.5, 2.0, 2.5, 3.0, 3.5, and 4.0 mM. In panel (b) curves (i) → (iii) correspond to [CTAB] = 0.0, 0.75, and 1.25 mM. In panel (c) curves (i) → (vii) correspond to [TX-100] = 0.0, 0.022, 0.044, 0.088, 0.13, 0.18, and 0.26 mM.

dx.doi.org/10.1021/jp304280m | J. Phys. Chem. B 2012, 116, 9704−9717

ports,[20,22,23,32,33] the two absorption bands at ~348 nm and ~370 nm for HM in aqueous buffer are attributed to the neutral and cationic species of HM (Scheme 1), respectively.

The relative intensity of the two absorption spectral bands is sensitive to the properties of the surrounding environments (e.g., nature of the solvent as well as externally added additives).[20,22,23,32,33] Figure 1a reveals a discernible modification of the absorption profile of the drug HM with increasing concentration of anionic surfactant SDS in terms of considerable broadening of the spectral profile with concomitant increase of absorbance for the cationic species ($\lambda_{abs} \approx 370$ nm). However, the modification on absorption profile of the drug in the presence of the cationic (CTAB, vide Figure 1b) and neutral (TX-100, vide Figure 1c) surfactants bears a noticeable inconformity to the observations in the presence of the anionic surfactant (SDS). As seen in Figure 1, panels b and c, the addition of cationic or neutral surfactant to the aqueous buffer solution of the drug (HM) results in distinct enhancement of the absorbance of the neutral band ($\lambda_{abs} \approx 348$ nm) relative to that of the cationic counterpart ($\lambda_{abs} \approx 370$ nm). Such modulations of the absorption spectra of HM are clear indications that the prototropic equilibrium of HM (Scheme 1) is enormously modified in the microheterogeneous environments of the surfactants compared to that in aqueous buffer phase.[20,22,23,32,33] It is thus argued that the ground-state prototropic equilibrium of HM is more favored to the neutral species in the presence of the cationic or neutral surfactants.

Given the cationic surface charge of CTAB it is not unlikely that the ground-state neutral ↔ cation prototropic equilibrium of the drug (HM) is favored more to the neutral species in the presence of this surfactant molecule (vide Figure 1b). However, a similar pattern of observation in the presence of the neutral surfactant TX-100 (vide Figure 1c) is noteworthy, and it is argued, in the present conjecture, that a decrease of medium polarity in the presence of the surfactants appears to play a key role in modulating the prototropic equilibrium of HM within the microheterogeneous micellar assemblies. However, the case of anionic surfactant appears a little puzzling at the moment. The anionic surface charge of the SDS surfactant molecule can be presumed to stabilize the cationic species of HM over the neutral species which should be manifested through a gradual increase of the cationic absorption band at $\lambda_{abs} \approx 370$ nm at the cost of the neutral counterpart at $\lambda_{abs} \approx 348$ nm with increasing anionic surfactant concentration.[34] However, the appreciable broadening of the absorption profile in the present case with increasing SDS concentration (vide Figure 1a) obscures such a clear distinction and hence invokes complications in quantitative evaluation of the spectral band features. Herein, we endeavor to resolve the problem by deconvolution of the experimental spectra into individual Gaussian curves following the method described in section 2.2. For the resolutions, the half-width values and peak maxima were varied slightly on a trial and error basis to obtain the best fit with a minimum in the goodness fit parameter χ^2 and a visual inspection of the superposition of the convoluted curves on the experimentally obtained spectra.[31] The results of deconvolution of the absorption profile of the drug (HM) in aqueous buffer medium and in the presence of different surfactants are systematically presented in Figure 2. For HM in aqueous buffer medium, Gaussian resolution of the absorption spectrum yields two bands corresponding to the neutral ($\lambda_{abs} \approx 348$ nm) and the cationic ($\lambda_{abs} \approx 370$ nm) species of the drug (Figure 2a). The Gaussian resolution of the experimental absorption spectrum of

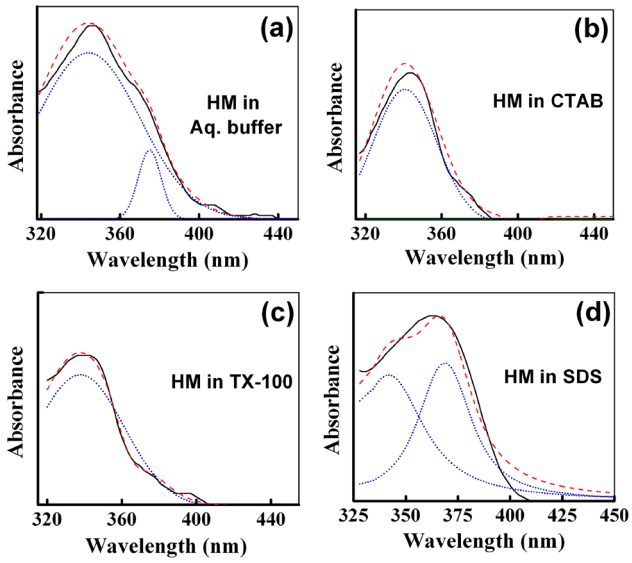

Figure 2. Resolved absorption spectra of HM in (a) aqueous buffer solution, (b) 0.8 mM CTAB, (c) 0.40 mM TX-100, and (d) 6.0 mM SDS. The black lines denote the experimental spectra, the blue dotted lines denote the resolved bands into the individual Gaussian components, and the red dashed lines designate the simulated spectra based on the resolved bands.

the drug in the presence of a substantial concentration of the cationic ([CTAB] = 1.25 mM, Figure 2b) or neutral ([TX-100] = 0.26 mM, Figure 2c) surfactant corroborates to the predominance of the absorption band of the neutral species at $\lambda_{abs} \approx 348$ nm only. This observation in turn appears to account for the aforementioned inference that in the presence of the cationic (CTAB) or neutral (TX-100) surfactant the ground-state prototropic equilibrium of HM is favored to the neutral species over the cationic counterpart. However, the case of anionic surfactant (SDS) produces interesting results. Deconvolution of the absorption spectrum of HM in the presence of the anionic surfactant ([SDS] = 4.0 mM) distinctly reveals the presence of two resolved bands corresponding to the neutral ($\lambda_{abs} \approx 348$ nm) and the cationic ($\lambda_{abs} \approx 370$ nm) species of HM, as displayed in Figure 2d. This finding thus points out the fact that even in the presence of a substantial concentration of the anionic surfactant the ground-state prototropic equilibrium of the drug is not completely moved to the cationic species, as is advocated by the presence of a significant contribution from the neutral absorption band (vide Figure 2d). It is thus logical to argue at this stage that the surface charge of the surfactant molecules is not the sole factor in governing the ground-state prototropic equilibrium of HM within the microheterogeneous assemblies of the micellar systems investigated. An interpretation for the significant contribution from the neutral absorption band of HM even in the presence of a substantial concentration of the anionic surfactant thus requires consideration of other factors as argued in forthcoming discussions.

However, the present score of observations also demands the consideration of other relevant factors, e.g., degree of water penetration in the micellar environments, local pH at the micellar surface, and micellar aggregation number. It is known that water can penetrate micellar units up to a certain depth depending on the compactness of the micellar units.[35,36] Berr et al. have demonstrated by neutron-scattering experiments that compactness of the micelle headgroup increases with increase

dx.doi.org/10.1021/jp304280m | J. Phys. Chem. B 2012, 116, 9704−9717

of surfactant chain length.[37] Micelles with smaller headgroups such as SDS experience a smaller degree of water penetration in comparison to micelles with larger headgroups such as CTAB and TX-100.[35,36] Thus a smaller degree of water penetration (micellar hydration) with SDS micelle as compared with CTAB and TX-100 micelles is expected to favor the prototropic equilibrium of HM toward the cationic form in CTAB and TX-100, which does not conform to the experimental results. Thus the model of water penetration (micellar hydration) which fails to account for the experimental observations is negated to play an important role. Another possible factor governing the prototropic equilibrium of HM between the neutral and cationic forms may be ascribed to the change of local pH at the micellar surface. However, the use of aqueous buffered solution at pH 7.40 is supposed to resist the change of pH of the solution and hence the local pH near the micellar surface. Recently Chakraborty et al.[38] explained this issue using nonsteroidal anti-inflammatory drugs of the oxicam family as chromophores in micelles of opposite charge (CTAB as cationic micelle and SDS as anionic micelle). They ascribed their observation of mutual transformation between the different prototropic species of the drugs to a change in the apparent pK_a values of the drugs. They considered the ionic interaction of the surfactant with the different prototropic species of the probe and the hydrophobic interaction between the nonpolar region of the micelles and the probe to be possible reasons for the apparent shift in the resulting pK_a values. Rottman and Avnir have also assigned a similar interpretation while explaining their experimental observation with a single dopant in micelles induced by additional sol−gel entrapment.[39] However, the role of the aggregation number and the size of the three micelles studied within our experimental window cannot be ruled out. For the presently investigated micellar systems, the aggregation number follows the trend: TX-100 (N_{agg} = 143[40]) > CTAB (N_{agg} = 92[41]) > SDS (N_{agg} = 60[42]). An increase in the aggregation number results in an increase in the surface charge of the micellar units which can subsequently influence the prototropic equilibrium of the drug.

Next, we contemplate the modifications of the emission spectral profile of HM upon interaction with the micellar systems. The emission profile of HM in aqueous buffer is comprised of a single unstructured broad band at $\lambda_{em} \approx 435$ nm, which is ascribed to the cationic species.[20,22,23,32,33] As displayed in Figure 3a, the cationic fluorescence of the drug undergoes discernible emission intensity enhancement following addition of the anionic surfactant (SDS). However, more dramatic modification on emission profile can be noticed upon addition of the cationic (CTAB, vide Figure 3b) and neutral (TX-100, vide Figure 3c) surfactants to the aqueous buffer solution of the drug in terms of prominent quenching of the cationic fluorescence band at $\lambda_{em} \approx 435$ nm with concomitant enhancement of a new fluorescence band at $\lambda_{em} \approx 375$ nm emanating from the neutral form of HM (Scheme 1).[20,22,23,32,33] Here also the model of water penetration (micellar hydration)[35,36] fails to account for the observed emission spectral changes. A less compact arrangement of the micellar headgroups for CTAB and TX-100 compared to SDS should be viable to penetration of water molecules to a greater extent in the former cases and should consequently favor the prototropic equilibrium toward the cationic form of HM because of an enhanced polarity. Evidently the experimental findings do not correlate to the expectation as deduced from the water penetration model.

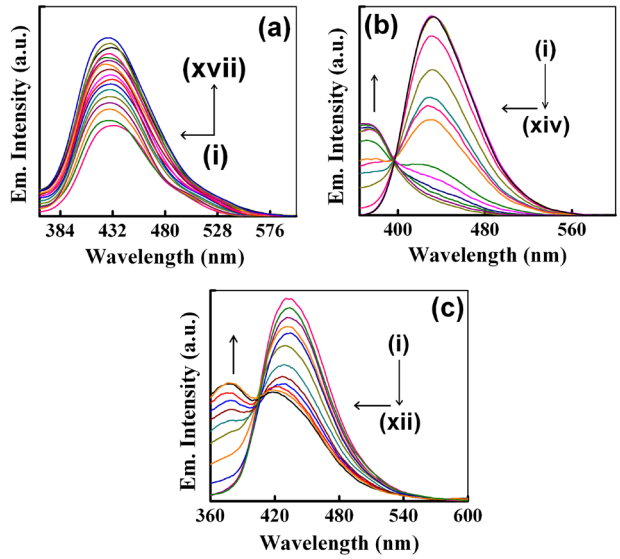

Figure 3. Representative emission spectral profile of HM (λ_{ex} = 350 nm) in aqueous buffer medium in the presence of increasing concentrations of (a) SDS, (b) CTAB, and (c) TX-100. In panel (a) curves (i) → (xvii) correspond to [SDS] = 0.0, 0.5, 1.0, 1.5, 2.0, 2.5, 3.0, 3.5, 4.0, 4.5, 5.0, 5.5, 6.0, 6.5, 7.0, 7.5, and 8.0 mM. In panel (b) curves (i) → (xiv) correspond to [CTAB] = 0.0, 0.1, 0.2, 0.3, 0.4, 0.6, 0.8, 0.9, 1.0, 2.0, 3.0, 4.0, 5.0, and 7.0 mM. In panel (c) curves (i) → (xii) correspond to [TX-100] = 0.0, 0.022, 0.044, 0.088, 0.13, 0.18, 0.22, 0.26, 0.31, 0.35, 0.40, and 0.44 mM.

Similarly, following the same line of argument as discussed above the change of local pH at the micellar surface is not believed to play an important role in governing the prototropic transformation of the drug in an aqueous buffered solution. Invalidating all these plausible considerations, we are thus left with the postulate of the degree of probe penetration into the micellar assemblies and the micellar compactness to rationalize the experimental findings.[43,44] Micelles with compact headgroups such as SDS should be vulnerable to allow only a smaller extent of probe penetration as compared with micelles with less compact headgroup arrangement (e.g., CTAB and TX-100[35−37]) in which the probe molecules are expected to be incorporated relatively deeper inside. This in turn delineates the enhancement of population of the neutral species of HM (reduced polarity) at the cost of the cationic counterpart with increasing concentration of CTAB or TX-100 surfactants (vide Figure 3, panels b and c). In harmony with these arguments, it is important to note here that the substantial enhancement of the cationic emission of HM in the anionic micellar environment (SDS) points out that the species (cationic form of the drug HM) probably does not penetrate deep into the micellar core; rather it is localized in the micellar interface region where it is likely to be stabilized (the results of Cu^{2+}-ion induced fluorescence quenching experiment, to be discussed in a forthcoming section, also approves this conjecture). It is also noted that the cationic fluorescence band of HM is slightly blue-shifted in the presence of the surfactants as compared to that in aqueous buffer phase (vide Figure 3a). This indicates lowering of polarity around the drug microenvironment in the micellar microheterogeneous environments in comparison to bulk aqueous buffer phase. This issue has been further substantiated in a forthcoming discussion.

Herein, in order to obtain a distinct visual comparison of the band features obtained on emission profile of HM in the

dx.doi.org/10.1021/jp304280m | J. Phys. Chem. B 2012, 116, 9704−9717

presence of various surfactants, the experimental spectra are deconvoluted into individual Gaussian curves. For HM in aqueous buffer, Gaussian resolution of the emission spectrum yields only one prominent band corresponding to the cationic species of HM at $\lambda_{em} \approx 435$ nm as displayed in Figure 4a.

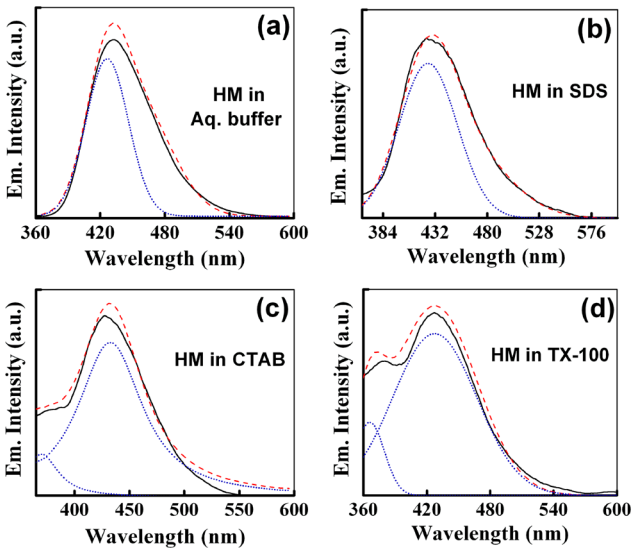

Figure 4. Resolved emission spectra of HM in (a) aqueous buffer solution, (b) 6.0 mM SDS, (c) 0.8 mM CTAB, and (d) 0.40 mM TX-100. The black lines denote the experimental spectra, the blue dotted lines denote the resolved bands into the individual Gaussian components, and the red dashed lines designate the simulated spectra based on the resolved bands.

Similar is the observation for resolution of the emission spectrum of HM in the presence of substantial concentration of the anionic surfactant ([SDS] = 4.0 mM, Figure 4b) (It is to note in this context that attempts to deconvolute the experimental spectra displayed in Figure 4, panels a and b, into multiple band features (with particular emphasis on the neutral ($\lambda_{em} \approx 375$ nm) and cationic ($\lambda_{em} \approx 435$ nm) emission bands of HM did not produce physically rational or acceptable results, as consistent with our arguments)). Whereas deconvolution of the experimentally obtained emission profile of HM in the presence of the cationic ([CTAB] = 1.25 mM, Figure 4c) or neutral ([TX-100] = 0.26 mM, Figure 4d) surfactant clearly reveals the resolved band features corresponding to the emission of the neutral form of HM at $\lambda_{em} \approx 375$ nm and the cationic form at $\lambda_{em} \approx 435$ nm.

In this context, a direct comparison of the emission spectral results with the absorption spectral results also points toward the differential modulation of the prototropic equilibrium of HM in the presence of the anionic surfactant (SDS) in the ground and excited-states.

It is seen from the absorption and emission spectral profiles of HM in cationic and neutral micellar environments that the neutral form of HM predominates in the ground-state, whereas in the emission profile, it also indicates the existence of the cationic form. This indicates the operation of the excited-state proton transfer process within the molecular system. This observation, in tune with the usual observations in connection with excited-state proton transfer reaction,[45] may be rationalized on the ground of relative energy barriers for the proton transfer process in the ground and excited electronic state. Usually the proton transfer reaction in the ground-state is argued to be disfavored by a high energy barrier, whereas a lowering of the energy barrier in the excited-state surface is not unlikely to promote an excited-state proton transfer process following electronic excitation.[45] Subsequently in the presence of the cationic and neutral micelles an enhancement of the neutral emission with concomitant decrease of the cationic emission indicates that the excited-state proton transfer process (the cation ↔ neutral prototropic equilibrium) of HM is favored toward the neutral species in these environments. This is consistent with the observations on the absorption profile which indicate lesser amount of the ground-state cationic species in the specified micellar environments leading to relatively lower intensity of the cationic fluorescence of HM on the emission profile.

3.2. Steady-State Fluorescence Anisotropy. Measurement of fluorescence anisotropy (r) is important since it provides fruitful information about the physical characteristics and the nature of the environments around the fluorophore.[6−11,20,22,23,30,46] Any factor affecting the size, shape and segmental flexibility of a fluorophore will get manifested through the observed anisotropy.[6−11,20,22,23,30,46] As depicted in Figure 5, an increase in anisotropy of HM with increasing

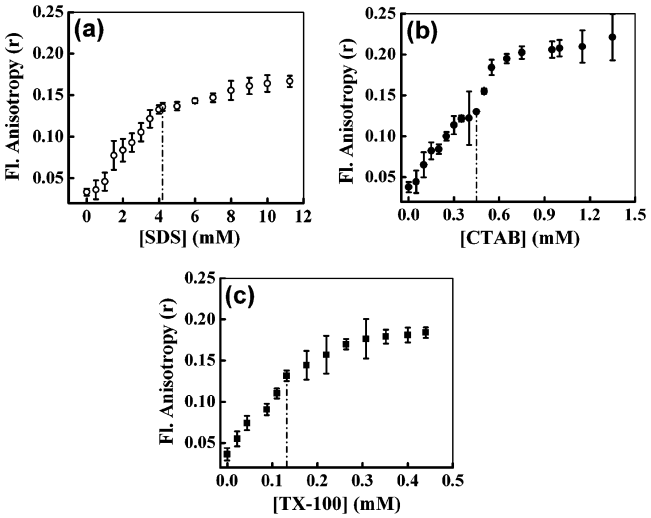

Figure 5. Variation of steady-state fluorescence anisotropy of HM with increasing concentration of (a) SDS (−○−), (b) CTAB (−●−), and (c) TX-100 (−■−) in Tris-HCl aqueous buffer. $\lambda_{ex} = 350$ nm and $\lambda_{em} = 430$ nm. Each data point is an average of 12 individual measurements. The error bars are within the marker symbols if not apparent. The breakpoints observed at the corresponding CMCs of the surfactants in Tris-HCl aqueous buffer solution are marked in each panel.

surfactant concentration indicates that the fluorophore experiences a motionally confined environment within the micelle-bound state compared to that in aqueous buffer medium. A steep rise in the fluorescence anisotropy of HM as a function of the surfactant concentration is found to be followed by attainment of a plateau region probably suggesting the saturation of interaction of the drug with the surfactants. A reasonably high value of anisotropy of HM at the saturation level of interaction suggests that the drug molecule experiences substantially rigid environment within the micellar assemblies. Also it is worth noting in the present context that the steady-state fluorescence anisotropy value (r) of the drug at the saturation level of interaction with different surfactants is not

dx.doi.org/10.1021/jp304280m | J. Phys. Chem. B 2012, 116, 9704−9717

equal and hence delineates the differential degrees of motional restriction imparted on the drug molecule in different micellar assemblies. Following the same line of argument as discussed above (section 3.1), the extent of probe penetration into the micellar units can be invoked to rationalize this observation. Micelles with smaller headgroups (e.g., SDS) ensures a more compact arrangement which in consequence allows relatively lesser degree of probe penetration into the micellar assemblies as against the case of micelles with larger headgroups (e.g., CTAB and TX-100) incorporating the probe molecules into a deeper inside.[34−36] Thus the microenvironment in the immediate vicinity of the probe molecule is expected to be more rigid and less polar in the cationic (CTAB) and neutral (TX-100) micelles in comparison to that in the anionic counterpart (SDS). This accounts for a larger magnitude of fluorescence anisotropy of HM in CTAB and TX-100 micellar assemblies compared to that in SDS at the saturation level of interaction (vide Figure 5).

It is interesting to note at this stage that the variation of steady-state fluorescence anisotropy (r) of the drug as a function of the surfactant concentration follows a specific pattern. A close perusal of Figure 5 reveals a breakpoint in the pattern of variation of fluorescence anisotropy in the vicinity of respective CMC values of the surfactants in aqueous buffer (Tris-HCl buffer, pH 7.40) medium. The CMC values of the surfactants thus estimated from Figure 5 are collected in Table 1 and found to juxtapose well with reported literature.[47−49] It is, however, pertinent here to underscore that we employ the variation of fluorescence anisotropy (r) of the probe with surfactant concentration as the actuating tool for estimation of the CMCs, instead of more conventionally applied technique of using the variation of fluorescence intensity of a fluorophore. In the course of verifying the applicability of different photophysical parameters of the probe in this respect, we found that the complex nature of the variation of fluorescence intensity of HM with varying surfactant concentrations (section 3.1, Figure 3) is not an appropriate choice for precisely locating the CMCs. Conversely, the pattern of variation of fluorescence anisotropy (r) emanated to be an efficient tool in pointing out the respective CMCs of the surfactants studied.

Table 1. Micellar Parameters of SDS, CTAB, and TX-100 in Aqueous Buffer Medium (Tris-HCl Buffer, pH 7.40) and Drug (HM)−Micelle Binding Parameters

environment	N_{agg}[a]	CMC[b] (mM)	r_h[c] (Å)	refs	K[d] (±10%) × 10^{-3} (M^{-1})	ΔG[e] (kJ mol^{-1})
SDS	60	4.20	20.7	40, 47	4.89	−21.19
CTAB	92	0.41	25.7	41, 48	30.39	−25.74
TX-100	143	0.13	44.0	40, 49	94.44	−28.57

[a]Aggregation number (N_{agg}) of the micellar systems. [b]Critical micellar concentration (CMC) values of the surfactants in aqueous buffer medium. [c]Hydrodynamic radius. [d]Drug (HM)−micelle binding constant (K). [e]Free energy change (ΔG) for the drug (HM)−micelle binding process at the experimental temperature (T = 300.0 K).

3.3. Drug−Micelle Binding. A quantitative assessment for the drug−micelle binding interaction can be derived in terms of evaluation of the binding constant (K) and the free energy change (ΔG) for the binding process. The estimation of binding constant rests on an analysis of the fluorescence intensity data of the drug (since the fluorescence intensity of HM differs significantly upon interaction with the studied micellar systems) following the method described by Almgren et al.[44] in which the binding constant (K) is expressed through the following relationship:

$$\frac{1}{I_x - I_0} = \frac{1}{I_\infty - I_0} + \frac{1}{K[\mathrm{M}]} \quad (5)$$

in which I_0, I_x, and I_α designate respectively the fluorescence intensity of the drug in the absence of surfactant, at an intermediate concentration of surfactant, and under conditions of saturation of interaction.

The micellar concentration [M] is given as

$$[\mathrm{M}] = \frac{[\mathrm{S}] - \mathrm{CMC}}{N_{agg}} \quad (6)$$

in which [S] represents the surfactant concentration, CMC is the critical micellar concentration, and N_{agg} is the aggregation number of the surfactant under consideration. The values of N_{agg} and CMCs are collected in Table 1.

Figure 6 displays the $1/[I_x - I_0]$ vs $1/[\mathrm{M}]$ plots for HM in the three different micellar environments and the binding constant values have been calculated from the intercept to slope ratio of the respective plots following eq 5, and the free energy change (ΔG) for the drug−micelle binding process has been subsequently calculated from the relationship $\Delta G = -RT \ln K$.

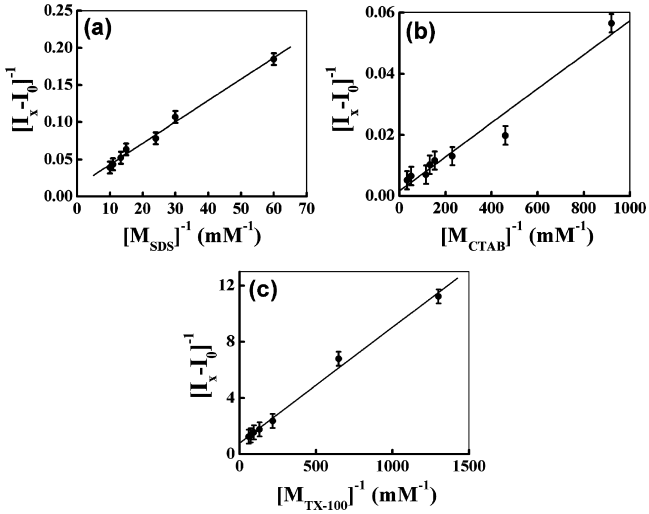

Figure 6. Plot of $[I_x - I_0]^{-1}$ vs $[\mathrm{M}]^{-1}$ (mM^{-1}) in (a) SDS, (b) CTAB, and (c) TX-100 for determination of drug−micelle binding constant.

The data compiled in Table 1 reveals the thermodynamic feasibility of the drug−micelle binding interaction process in all three cases under investigation through a negative free energy change.[6,7,22,23,30,42,44] Of particular interest in this context is to note the relative order of magnitude of the binding constants in various micellar assemblies. The data collected in Table 1 evince the same order of drug−micelle binding constant with the cationic (CTAB) and neutral (TX-100) micelles, whereas it is clearly 1 order of magnitude lower with the anionic micelle (SDS). Apparently a lower magnitude of binding constant of the cationic probe (HM) with the anionic micelle (SDS) in comparison to the cationic (CTAB) or neutral (TX-100) counterparts appears to contradict our usual expectations based on electrostatic stabilization of the interaction between cationic drug (HM) and anionic micelle (SDS). However, the results can be rationalized in terms of the aforementioned postulate of

dx.doi.org/10.1021/jp304280m | J. Phys. Chem. B 2012, 116, 9704−9717

degree of probe penetration into the micellar units (as discussed in sections 3.1 and 3.2). Incorporation of the probe molecules into a deeper inside the cationic and neutral micelle should conform to a more compact arrangement of the probe molecules after interaction with the micellar units as compared with the anionic micelle which allows lesser degree of probe penetration (also in anionic micellar environment the cationic species of the drug is likely to be stabilized out of favorable electrostatic interaction whence the cationic drug is argued to be preferably localized at the micellar interfacial region rather than penetrating deep into the micellar core).[6,34−36] Thus the results of the drug−micelle binding constant (vide Table 1) are found to correlate well to the steady-state anisotropy data as discussed in the previous section.

3.4. Polarity of the Micellar Microenvironment: Assessment of the Probable Location of the Drug. The precise determination of microscopic polarity of biological and biomimicking assemblies is an important goal in biological and biochemical research. Environment sensitive photophysical properties of fluorescent probes have been employed in serving this purpose since a couple of decades.[7,20,22,23,34,46,50] The local polarity of the drug binding site on the micelle can be estimated by comparing the spectral properties of the drug in the environment with those in pure solvent or solvent mixture of known polarity. Although the polarity of a microheterogeneous environment is not exactly the same as that of a homogeneous fluid, a relative estimate of the micropolarity around the fluorophore generally yields reliable results.[7,20,22,23,34,46,50] This polarity has been referred as the static polarity by Sytnik and Kasha.[51] The medium polarity-sensitive prototropic transformation of HM has formed the actuating basis in this study. The fluorescence behavior of HM has been monitored in varying compositions of water−1,4-dioxane mixture of known polarity and is displayed in Figure 7a. It is seen that decreasing

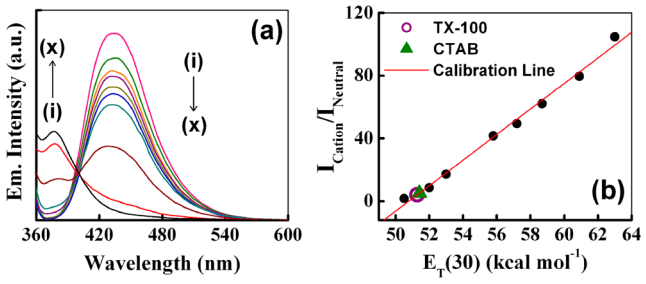

Figure 7. (a) Emission profile of HM in varying composition of water-dioxane mixture (λ_{ex} = 350 nm). Curves (i) → (x) correspond to % dioxane (by volume) = 0, 10, 20, 30, 40, 50, 60, 70, 80, and 90. (b) Construction of calibration curve for micropolarity determination by plotting the ratiometric variation of emission intensities of the cationic to neutral species of HM ($I_{Cation}/I_{Neutral}$) as a function of polarity equivalent parameter, $E_T(30)$ (in kcal/mol) of reference solvent mixtures of water-dioxane. The micropolarity of HM interaction site in CTAB (−▲−, green) and TX-100 (−○−, purple) micellar systems are indicated in the figure.

polarity of the medium (increasing the dioxane proportion in the water/1,4-dioxane solvent mixture) is associated with a regular depletion of the cationic fluorescence with concomitant emergence of a new band at $\lambda_{em} \sim 375$ nm corresponding to the neutral species of HM (Scheme 1).[20,22,23,32,33] The consequent increasing degree of destabilization of the cationic species with decreasing medium polarity corroborates to this observation.[20,22,23,32,33]

The estimation of the polarity of drug microenvironment in micellar microenvironment has been rested on comparison of the fluorescence properties of the drug within the micellar systems to those observed in the reference solvent mixture. A calibration curve (in form of a linear regression) has been constructed by plotting the relative variation ($I_{Cation}/I_{Neutral}$) of cationic fluorescence intensity (I_{Cation} at $\lambda_{em} \approx 435$ nm) to that of the neutral form ($I_{Neutral}$ at $\lambda_{em} \approx 375$ nm) of HM in water−1,4-dioxane reference solvent mixture as a function of the polarity equivalent parameter, $E_T(30)$.[51,52] The same parameter $I_{Cation}/I_{Neutral}$ has been constructed for modulation of emission intensity of HM in the cationic (CTAB) and neutral (TX-100) micellar environments (with all experimental conditions and instrumental settings conserved) and interpolation of the value on the calibration curve leads to the micropolarity of the drug binding site in the micellar assemblies as to be 51.41 for CTAB and 51.29 for TX-100 on the $E_T(30)$ (in kcal mol^{-1}) scale (Figure 7b). Herein, ratiometric calibration scheme ($I_{Cation}/I_{Neutral}$) has been emphasized during estimation of the polarity in the immediate vicinity of the drug in micellar microheterogeneous environments as it is more fruitful as an actuating tool since it is independent of experimental and instrumental artifacts like fluctuations in probe concentration, excitation source intensity, light scattering, stability under illumination, and so forth, and hence is independent of the need of frequent calibration during estimation of the parameter.

The estimated values of micropolarity of the drug in the immediate vicinity of its interaction site within the micellar environments thus indicates a reduced polarity in comparison to that in aqueous buffer phase ($E_T(30)$ = 63.1 kcal mol^{-1}). The values are also found to bear reasonable harmony to literature reports for the polarities of the Stern layer of the micellar systems as determined earlier using betaine dye,[53] 4-*N*,*N*′-dimethylamino-3-hydroxyflavone[54] and 1-anilino-8-naphthalene sulfonate.[55] The present results thus suggest that the drug molecule is probably localized in the Stern layer of the cationic and neutral micellar environments.

However, the same technique here cannot be applied for determination of micropolarity of the drug microenvironment within the anionic micelle (SDS) because the fluorescence profile of the drug in anionic micelle (vide Figure 3a) showing only one band corresponding to the cationic emission of HM cannot be paralleled to the observations illustrated in Figure 7a. Thus in order to cast light on the probable location of the probe in anionic micellar environment and also to reinforce the interpretations derived from the micropolarity measurement, the following strategy of externally modifying the fluorescence properties of HM in aqueous buffer and micelle-bound HM has been undertaken.

Fluorescence Quenching. In an endeavor to externally modify the fluorescence of micelle-bound HM we adopted the strategy of fluorescence quenching of the probe in different environments. This is a simple but efficient strategy for assessing the location of the probe within the micellar environments. The bromide (Br^-) or copper (Cu^{2+}) ion-induced fluorescence quenching of HM has been followed on the following Stern−Volmer equation[30]

$$\frac{I_0}{I} = 1 + K_{SV}[Q] \qquad (7)$$

dx.doi.org/10.1021/jp304280m | J. Phys. Chem. B 2012, 116, 9704−9717

in which I_0 is the original fluorescence intensity, I is the quenched intensity of the fluorophore (HM), [Q] is the molar concentration of the quencher and K_{SV} is the Stern–Volmer quenching constant. The higher the magnitude of K_{SV}, the more efficient is the quenching ensuring the greater is the degree of exposure of the quencher to the probe.[20,22,23,30,34,42] The Stern–Volmer plots for bromide and Cu^{2+} ion-induced quenching of HM in aqueous buffer and various micellar environments are displayed in Figure 8, panels a and b,

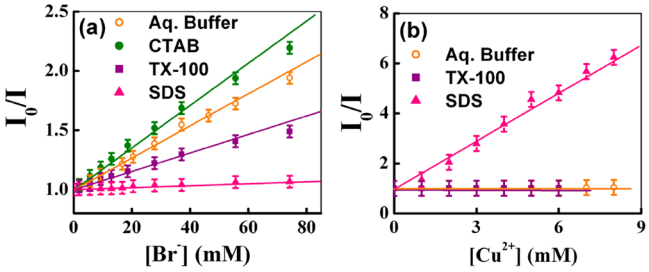

Figure 8. Stern–Volmer plot for (a) bromide ion (Br^-) and (b) Cu^{2+} ion-induced fluorescence quenching of the drug (HM) in aqueous buffer (–○–; orange), 0.80 mM CTAB (–●–; green), 0.31 mM TX-100 (–■–; purple), and 6.0 mM SDS (–▲–; pink) micellar environments.

respectively. The negatively charged Br^- ion is found to be an efficient quencher for HM (Figure 8a) corresponding to K_{SV} (±10%) = 12.89 M^{-1}. However, on performing the same quenching experiment on micelle-encapsulated probe (with all experimental conditions and instrumental settings conserved), the extent of quenching is found to be noticeably modified (vide Figure 8a, Table 2). The quenching efficiency becomes

Table 2. Fluorescence Quenching Data for HM in Aqueous Buffer and Micellar Media

environment	quencher	K_{SV} (±10%) (M^{-1})
aqueous buffer	Cu^{2+}	5.07
	Br^-	12.89
SDS	Cu^{2+}	687.4
	Br^-	1.01
CTAB	Cu^{2+}	
	Br^-	16.18
TX-100	Cu^{2+}	1.15
	Br^-	6.72

minimum for HM bound to anionic micelle (SDS), and maximum for HM bound to cationic micelle (CTAB) while in the neutral micellar environment (TX-100) the quenching efficiency is intermediate between those observed in bulk aqueous buffer and anionic SDS micelle (vide Figure 8a, Table 2). This scenario is readily understandable since in SDS micelle the repulsive electrostatic interaction between the negative surface charge of the micelle and that of the quencher (Br^- ion) should ensure considerable lowering of the quenching efficiency by resisting a close accessibility of the quencher to the fluorophore, while the reverse situation should prevail in the cationic micellar environment (CTAB) accounting for an enhanced quenching efficiency.[20,22,23,30,34,42]

In order to further substantiate the results of Br^- ion-induced quenching experiment, the fluorescence quenching experiment has also been performed with a cationic quencher viz., Cu^{2+} ion. The results of Cu^{2+} ion-induced fluorescence quenching on HM in aqueous buffer and in various micellar environments are found to follow a qualitatively reverse pattern with respect to those observed during Br^- ion-induced quenching (vide Table 2, Figure 8b). The positively charged quencher (Cu^{2+} ion) is found to be a feeble quencher for the cationic probe molecule HM (K_{SV} (±10%) = 5.07 M^{-1}) as can be rationalized on the lexicon of electrostatic repulsion between the like charges of the probe and the quencher resisting a close approach between the concerned partners. Whereas in anionic micellar environment the Cu^{2+} ion-induced quenching efficiency is found to be remarkably enhanced (vide Table 2) presumably owing to high local concentration of the quencher ions near the surface because of electrostatic attraction and thereby ensuring a close accessibility of the quencher to the probe.[20,22,23,30,34,42]

Cumulatively, the results of cationic (Cu^{2+} ion) and anionic (Br^- ion) quencher induced fluorescence quenching experiments of HM in aqueous buffer and different micelle-encapsulated state demonstrate that the probe does not penetrate deep into the micellar hydrophobic core region, which is characterized by highly viscous hydrocarbon-like environment.[20,22,23,30,34,42] For otherwise, had the probe been located in the hydrophobic core of the micelles none of the ionic quenchers could have been expected to impart discernible modulation in the extent of quenching depending on the microheterogeneous environment of the probe as the hydrophobic micellar core region should have restricted the penetration of the ionic quencher.[56]

3.5. Wavelength-Sensitive Fluorescence Behavior: The Red-Edge Excitation Effect. A wavelength sensitive tool for directly monitoring the environment and dynamics around a fluorophore in a complex microheterogeneous system and the solvation dynamics in an organized medium is the red-edge excitation shift or REES, i.e., the shifting of the emission maxima to the red end of the spectrum upon shifting of the excitation wavelength to the red end of the absorption spectrum of the fluorophore.[6,7,20,23,30,57,58] Here we have monitored the dependence of emission maxima of HM on excitation wavelength in the presence of different surfactants and the results are displayed in Figure 9a along with a representative case showing the occurrence of REES with CTAB-bound micelle in Figure 9b. The occurrence of excitation-wavelength dependence is connected to the presence of ensembles of molecules in the ground-state differing in their solvation sites and hence energies.[57,58] Precisely, the operation

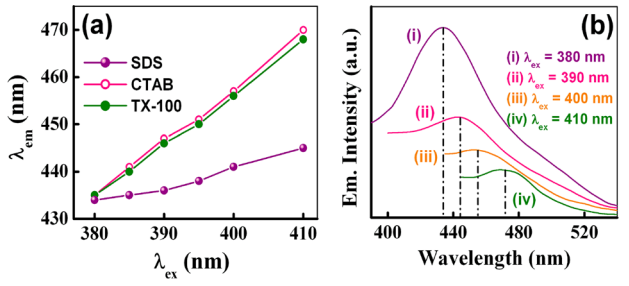

Figure 9. (a) Red-Edge Excitation Shift (REES) profile for HM in the presence of varying surfactant concentrations as specified in the figure legend. The REES profile is described in terms of shifting of the emission maxima to the red upon shifting of the excitation wavelength to the red end of the absorption spectrum. (b) A representative case for the occurrence of REES in micelle-bound drug (HM) for [CTAB] = 0.80 mM.

dx.doi.org/10.1021/jp304280m | J. Phys. Chem. B 2012, 116, 9704–9717

of REES is subject to the following conditions: (a) there should exist a distribution of solute−solvent interaction energy leading to inhomogeneous broadening of the absorption spectra which subsequently will allow the provision of site photoselection of energetically different species. Such inhomogeneous broadening is shown to be particularly significant for molecules having a greater dipole moment in the excited-state than in the ground-state, and is described by a simple expression according to Onsager sphere approximation:[57]

$$\Delta\nu = A\Delta\mu\rho^{-3/2}(k_B T)^{1/2} \quad (8)$$

Here A is a constant that depends on the dielectric constant of the medium, ρ is the Onsager cavity radius, k_B is the Boltzmann's constant and $\Delta\mu$ is the change of dipole moment following excitation. However, additional broadening, which can play even a greater role in inhomogeneous broadening of absorption spectra, may be induced by specific interactions of the sort of hydrogen bonding, electrostatic interactions and so forth.[57,58] (b) Second, the solvent molecules around the fluorophore must be polar and the solvent reorientation time ($\langle\tau_{solvent}\rangle$) should be slower or comparable to the fluorescence lifetime (τ_f) of the fluorophore so that unrelaxed fluorescence can give rise to excitation-wavelength-dependent emission behavior.

Figure 9a illustrates that the shift of excitation wavelength from 380 to 410 nm resulting in shift of the emission maxima of the probe to the red.[59] The effect is seen in a general manner for a range of surfactant concentration, which suggests that binding of the probe to the micelles offers restriction to the rotation of solvent dipoles around the excited fluorophore. Furthermore, given the complex microheterogeneous nature of the micellar environments additional broadening of absorption spectra (as mentioned above) is not unlikely to contribute to the operation of REES in the present case.[6,7,20,23,30,57,58]

In a nut-shell, the present observations imply that binding of HM to the micellar systems causes considerable restriction to the orientation of solvent dipoles around the excited-state fluorophore. It is also interesting to note in the present context that a high degree of REES is observed for the drug in the cationic (CTAB) and neutral (TX-100) micellar environment as compared with the anionic micellar assembly (*vide* Figure 9a). This is not surprising given the probable location of the drug in the Stern layer of the micellar units in the former two cases (CTAB and TX-100) and in the micelle-water interfacial region in the latter (SDS) since the Stern layer of micellar systems is documented to be comprised of the micellar headgroup, counterion and largely structured water molecules.[12]

3.6. Dynamic Light Scattering. Dynamic light scattering (DLS) measurement provides an effective way to investigate the dimensions of macromolecular and supramolecular assemblies.[8,41,42,46] It estimates the diffusion coefficient from which the hydrodynamic radius of the particle (r_h) can be evaluated using the Stokes−Einstein−Debye (SED) equation assuming the assembly to be spherical.[8,41,42,46] In the present case the DLS profiles of the micellar systems investigated is found to yield fairly monomodal distribution (figures not shown) and the as-obtained hydrodynamic radii are appended in Table 1, which are found to juxtapose reasonably well with existing literature.[40−42,47−49] It is also noticed that addition of the probe to each of the micellar solutions could introduce hardly any change in the hydrodynamic radii.

3.7. Time-Resolved Fluorescence Decay. Fluorescence lifetime measurement serves as a sensitive and faithful indicator for exploring the local environment around a fluorophore.[6−9,20−23,30,46,60,61] It also exerts imperative contributions toward deciphering the excited-state interaction of the probe within the micellar microheterogeneous environments.[6,11,20,30,46,60,61] In order to deduce an elaborate analysis of the scenario we have monitored the fluorescence lifetime of HM in aqueous buffer medium and in the presence of a series of surfactant concentrations. The typical time-resolved fluorescence decay profiles are displayed in Figure 10 and the

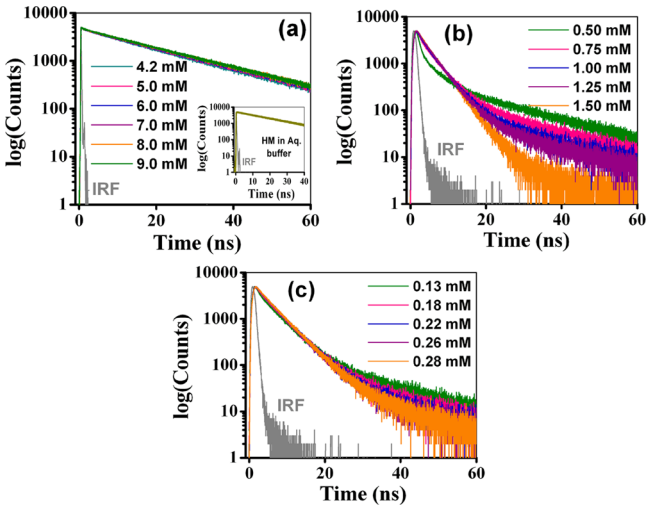

Figure 10. Representative time-resolved fluorescence decay profiles of HM in the presence of increasing concentrations of (a) SDS (λ_{ex} = 375 nm, $\lambda_{monitored}$ = 435 nm), (b) CTAB (λ_{ex} = 340 nm, $\lambda_{monitored}$ = 375 nm), and (c) TX-100 (λ_{ex} = 340 nm, $\lambda_{monitored}$ = 375 nm). The respective concentrations of the surfactants under investigation are specified in the figure legends. The inset of panel (a) displays the fluorescence decay curve of HM in aqueous buffer phase. The sharp gray profile on the extreme left of each panel indicates the instrument response function (IRF).

corresponding fitting parameters are compiled in Table 3. The drug molecule is found to exhibit a single-exponential decay pattern in bulk aqueous buffer phase with a lifetime of 21.67 ns.[20,22,23,33] The data summarized in Table 3 unveils that interaction with the micellar systems renders the time-resolved fluorescence decay of the probe to be multiexponential when a complicated multiexponential function was required to fit the data adequately. Such a behavior may, in principle, emanate from the differential distribution of the probe molecules in the micellar environments.[62−66] The data collected in Table 3 reflect that in anionic micellar environment the fluorescence decay behavior (λ_{ex} = 375 nm, λ_{em} = 435 nm) is described by a biexponential decay pattern comprising of a longer lifetime and a relatively shorter ultrafast component. In the micellar environments, the longer-lived component has a lifetime closely resembling to that of the probe in aqueous buffer medium whereas the shorter component is significantly different. Observation of two widely different time constants in the fluorescence decays implies the existence of two dynamical processes that occur on different time scales. One obvious possibility to decipher the origin of a slow and a fast component in the fluorescence decay may be intertwined with the distribution of the drug in the bulk aqueous buffer phase and in the micelles, respectively. However, in order for this

dx.doi.org/10.1021/jp304280m | J. Phys. Chem. B 2012, 116, 9704−9717

Table 3. Time-Resolved Fluorescence Decay Parameters for HM in Aqueous Buffer (Tris-HCl Buffer, pH 7.40) and Micellar Environments

environment	τ_1 (ns)	τ_2 (ns)	τ_3 (ns)	α_1	α_2	α_3	χ^2	$\langle\tau_{i0}\rangle$ (ns)
aqueous buffer	21.67			1.00			1.09	21.67
				[SDS] (mM)				
4.2	19.53	0.947		0.88	0.12		1.06	19.40
5.0	20.32	0.969		0.89	0.11		1.04	20.21
6.0	20.75	0.818		0.90	0.10		1.00	20.66
7.0	20.93	0.824		0.90	0.10		1.02	20.84
8.0	21.12	0.830		0.91	0.09		1.06	21.04
9.0	21.27	0.968		0.92	0.08		1.04	21.19
				[CTAB] (mM)				
0.50	20.71	0.524	3.74	0.031	0.83	0.13	1.06	9.83
0.75	20.46	0.566	3.81	0.023	0.62	0.35	1.05	6.93
1.00	20.21	0.609	3.88	0.015	0.41	0.57	1.07	5.38
1.25	20.22	0.593	3.79	0.012	0.33	0.65	1.02	4.95
1.5	21.03	0.588	3.69	0.010	0.30	0.69	1.05	4.74
				[TX-100] (mM)				
0.13	20.71	0.556	4.86	0.02	0.54	0.44	1.02	6.71
0.18	18.72	0.555	4.87	0.017	0.43	0.55	1.01	5.92
0.22	16.74	0.555	4.87	0.014	0.32	0.667	1.00	5.42
0.26	16.24	0.594	4.88	0.013	0.28	0.70	1.00	5.33
0.28	15.53	0.599	4.87	0.012	0.24	0.74	1.11	5.21

proposition to be correct the ratio of the relative amplitudes, i.e., α_1/α_2, should have been corresponding to the ratio of free dye to the bound dye. In course of verifying the validity of this consideration, we have calculated the ratio of relative concentration of micelle-bound HM to that in aqueous buffer phase following the method described in the literature (by Fayer et al., ref 65) and the value is found to be enormously different from the ratio α_1/α_2 (calculation suggests that more than 95% dye is bound to micelle).[20,66] This result explicitly dictates that the observed fluorescence decay in the micellar environment can be entrusted only on the dynamics of the micelle-bound probe while negating any considerable contribution from the free (unbound) dye. Further, it is imperative to note in the present context (vide Table 3) that the lifetime of the cationic species (longer-lived component, τ_1 in Table 3) comprises the major component in the overall decay pattern and its relative amplitude is found to gradually increase with increasing concentration of the anionic surfactant, which can be understandably argued on the ground of stabilization of the cationic species in the anionic micellar environment.

The fluorescence decay behavior of HM in the presence of the neutral (TX-100) or cationic (CTAB) micelle (λ_{ex} = 340 nm, λ_{em} = 375 nm) is found to bear a discernible harmony with each other but differs from the findings in the presence of the anionic micelle (ca. Table 3). In the presence of the neutral or cationic micelle the fluorescence decay of the drug is found to be adequately described by a complicated triexponential function which dictates only a small contribution from the cationic species of HM (the longer-lived component, τ_1 in Table 3). It is also encouraging to note that increasing surfactant concentration (TX-100 and CTAB) accompanies gradual decrease of relative amplitude of the cationic species which can be argued to reflect decreasing degree of stabilization of the cationic species of the drug in neutral or cationic micelle environments. This pattern of observation is found to be in consensus with other experimental findings as discussed previously. Conversely, the relative increase in the amplitude of the comparatively shorter component is also noteworthy. At this juncture it appears logical to attribute this component to the neutral species of the drug which is progressively stabilized in the presence of increasing concentration of the neutral or cationic surfactant. This conjecture is further supported by the fluorescence lifetime of HM in bulk 1,4-dioxane medium (τ_f = 2.87 ns) which resembles the observed shorter component in the presence of the neutral and cationic surfactants (in bulk 1,4-dioxane medium the steady-state emission spectral profile of the drug represents the band due to the neutral species only, vide Figure 7). Monitoring the fluorescence decay behavior of the probe in cationic and neutral micelles at λ_{ex} = 375 nm and λ_{em} = 435 nm has been found to yield no significant difference in the fluorescence lifetime of the cationic species which is rather the minor component in the fluorescence decay pattern.

However, it is noteworthy that the fluorescence decay behavior of HM in micellar environments also reveals the presence of an ultrafast component. A precise assignment for this ultrafast decay component is lacking at this moment, however, keeping parity with many recent reports[62−65] it is not unlikely in a complex microheterogeneous assembly, in which the probe may also undergo complex or/and unequal hydration.

3.8. Rotational-Relaxation Dynamics: Time-Resolved Fluorescence Anisotropy Decay. The time-dependent decay of fluorescence anisotropy is a sensitive indicator of the rotational motion and/or rotational-relaxation of the fluorophore in an organized assembly.[8,9,20,23,30,56,67−69] Therefore, with a view to delve into the microenvironment in the immediate vicinity of micelle bound-drug, time-resolved fluorescence anisotropy decay has been recorded in the studied micellar environments. The typical anisotropy decay profile is displayed in Figure 11 and the relevant dynamic parameters are summarized in Table 4. The anisotropy decay is described by the following equation:[30]

$$r(t) = \sum_i \beta_i \theta_i \qquad (9)$$

dx.doi.org/10.1021/jp304280m | J. Phys. Chem. B 2012, 116, 9704−9717

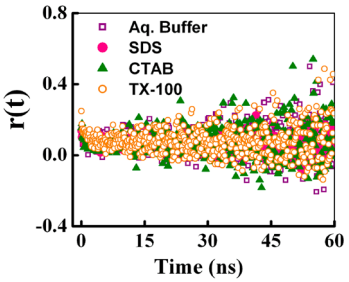

Figure 11. Typical time-resolved fluorescence anisotropy decay profile of HM in aqueous buffer (–□–; purple), 6.0 mM SDS (–●–; pink), 1.00 mM CTAB (–▲–; green), and 0.26 mM TX-100 (–○–; orange).

in which β_i designates the pre-exponential factor for the *i*th rotational correlation time, θ_i.

Table 4. Rotational Dynamical Parameters of HM in Aqueous Buffer (Tris-HCl Buffer, pH 7.40) and Micellar Environments

environment	β (%)	θ (ps)	χ^2	θ_M (ns)
aqueous buffer	100	124	1.00	
SDS	100	856	1.03	7.08
CTAB	100	882	1.10	13.7
TX-100	100	709	1.05	68.74

The rotational-relaxation time of the drug is found to be notably enhanced within the microheterogeneous micellar assemblies compared with that in bulk aqueous buffer phase confirming the signature for impartation of considerable degree of rigidity in the micellar microenvironments (vide Table 4). Further, that the rotational-relaxation time of the drug in all the studied micellar environments (vide Table 4) is faster than the corresponding fluorescence lifetimes in the same environment (vide Table 3) espouses that the excited-state fluorescence depolarization of the drug is essentially completed within the excited-state lifetime.

A single exponential decay function has been exploited to adequately describe the anisotropy decays of HM in aqueous buffer as well as micellar environments. Now, several arguments might emanate to account for the relaxation of the fluorescence anisotropy of the micelle bound-probe. The following possibilities are thus taken into consideration:[8,9,20,23,30,56,67−69] (i) the fluorophore rotates within the micelle; (ii) the entrapped fluorophore cannot rotate but the micellar unit carrying the probe rotates; and (iii) both rotations are possible.

The third option is immediately negated with a view to the observed single exponential anisotropy decay, since a biexponential decay pattern can only suitably interpret the possibility of both the rotations being operative. Now, in an endeavor to confirm one of the former two possibilities we have calculated the rotational-relaxation times of the micellar units (θ_M) according to the Stokes−Einstein−Debye (SED) relation:[8,9,30,56]

$$\theta_M = \frac{4}{3}\pi r_h^3 \frac{\eta}{k_B T} \quad (10)$$

Here, η is the coefficient of viscosity of the medium, r_h is the hydrodynamic radius of the micellar units (as obtained from DLS measurement and summarized in Table 1), k_B is the Boltzmann constant, and T is the Kelvin temperature. That the rotational-relaxation times of the micellar units are remarkably higher than the corresponding fluorescence depolarization times in respective environments leads to infer that the observed rotational-relaxation dynamics is attributable to the rotational motion of the probe only and not of the micellar units.[8,9,20,23,30,56,67,68]

4. CONCLUSIONS

The present work reports the study of interaction of a promising cancer cell photosensitizer HM with micellar assemblies of varying surface charges. The binding interaction of the drug with the micelles is found to be governed by a conjugate effect of polarity and rigidity of the micellar microheterogeneous environments. The results of steady-state and time-resolved fluorometric studies reveal the differential modulation of the prototropic equilibrium of the drug (HM) in micellar environments of varying surface charges. The results of micropolarity measurement at the drug interaction site within the micelles combined with the results of fluorescence quenching experiments delineate the probable location of the drug in the Stern layer of the cationic and neutral micellar systems whereas in the anionic micellar system the drug is probably localized in the micellar interfacial region. These results have been found to corroborate well to the steady-state fluorescence anisotropy data assessing the relative degrees of motional rigidity imparted on the drug molecule in different micellar environments. In direct context to these results the wavelength-sensitive fluorescence behavior of the micelle-bound drug also appears consistent. The pattern of drug−micelle binding constant and the free energy change of the interaction process are also found to be suitably rationalized on the lexicon of the relative degrees of penetration of the drug into micellar units in the context of probable location of the drug in various micellar environments.

Overall, given the enormous biological applications of β-carboline drugs and their promising prospects in many burgeoning research arenas, e.g., photodynamic therapy and so forth, the study of characterization of the strength and mode of binding interaction of such drug molecules with relevant biological and/or biomimicking receptors appear important. We are optimistic that the presently exploited experimental protocols and methodologies can be extended to other systems also.

AUTHOR INFORMATION

Corresponding Author

*Tel.: 91-33-2350-8386. Fax: +91-33-2351-9755. E-mail: nguchhait@yahoo.com.

Present Address

[§]Department of Chemistry and Biochemistry, University of Colorado at Boulder, Boulder, Colorado 80309, United States.

Author Contributions

[†]Equal contribution.

Notes

The authors declare no competing financial interest.

ACKNOWLEDGMENTS

B.K.P. thankfully acknowledges CSIR, India for Senior Research Fellowship, D.R. acknowledges UGC, India for Junior Research Fellowship. N.G. thanks DST, India for financial assistance through Project No. SR/S1/PC/26/2008.

REFERENCES

(1) Rekharsky, M. V.; Inoue, Y. *Chem. Rev.* **1998**, *98*, 1875−1917.
(2) Villalonga, R.; Cao, R.; Fragoso, A. *Chem. Rev.* **2007**, *107*, 3088−3116.
(3) Bodor, N. S. *Chemical Aspects of Drug Delivery Systems*; Karsa, D. R., Stephenson, R. A., Eds.; Royal Society of Chemistry: London, 1996.
(4) Xia, Y.; Rodgers, J.; Paul, K. E.; Whitesides, G. M. *Chem. Rev.* **1999**, *99*, 1823−1848.
(5) Hashimoto, S.; Thomas, J. K. *J. Am. Chem. Soc.* **1985**, *107*, 4655−4662.
(6) Paul, B. K.; Samanta, A.; Guchhait, N. *Langmuir* **2010**, *26*, 3214−3224.
(7) Paul, B. K.; Samanta, A.; Guchhait, N. *J. Phys. Chem. B* **2010**, *114*, 6183−6196.
(8) Paul, B. K.; Guchhait, N. *J. Phys. Chem. B* **2010**, *114*, 12528−12540.
(9) Paul, B. K.; Guchhait, N. *J. Colloid Interface Sci.* **2011**, *353*, 237−247.
(10) Rawat, S. S.; Kelkar, D. A.; Chattopadhyay, A. *Biophys. J.* **2005**, *89*, 3049−3058.
(11) Maiti, N. C.; Krishna, M. M.G.; Brito, P. J.; Periasamy, N. *J. Phys. Chem. B* **1997**, *101*, 11051−11060.
(12) (a) Tanford, C. *Science* **1978**, *200*, 1012−1018. (b) Pal, S. K.; Mandal, D.; Bhattacharyya, K. *J. Phys. Chem. B* **1998**, *102*, 11017−11023. (c) Sen, P.; Mukherjee, S.; Halder, A.; Bhattacharyya, K. *Chem. Phys. Lett.* **2004**, *385*, 357−361. (d) Kalyanasundram, K. *Photochemistry in Microheterogenous Systems*; Academic Press: New York, 1987.
(13) Bloom, H.; Barchas, J.; Sandler, M.; Usdin, E. *Progress in Clinical and Biological Research. Beta-carbolines and Tetrahydroisoquinolines*; Alan R. Liss Inc.: New York, 1982; Vol. *90*.
(14) Braestrup, C.; Nielsen, M.; Olsen, C. E. *Proc. Natl. Acad. Sci. U.S.A.* **1980**, *77*, 2288−2292.
(15) Carlini, E. A. *Pharmacol., Biochem. Behav.* **2003**, *75*, 112−116.
(16) Dolmans, D. E. J. G. J.; Fukumura, D.; Jain, R. K. *Nature Rev. Cancer* **2003**, *3*, 380−387.
(17) Henderson, B., Dougherty, T., Eds.; *Photodynamic Therapy: Basic Principles and Clinical Applications*; Marcel Dekker Inc.: New York, 1992.
(18) Reyman, D.; Pardo, A.; Poyato, J. M. L. *J. Phys. Chem.* **1994**, *98*, 10408−10411.
(19) Beljanski, M.; Beljanski, M. S. *Exp. Cell Biol.* **1982**, *50*, 79−87.
(20) Paul, B. K.; Guchhait, N. *J. Phys. Chem. B* **2011**, *115*, 10322−10334.
(21) Moulik, S. P. *Curr. Sci.* **1996**, *71*, 368−375.
(22) Paul, B. K.; Guchhait, N. *Photochem. Photobiol. Sci.* **2012**, *11*, 661−673.
(23) Paul, B. K.; Guchhait, N. *J. Phys. Chem. B* **2011**, *115*, 11938−11949.
(24) Yokoyama, M.; Kwon, G. S.; Okano, T.; Sakurai, Y.; Seto, T.; Kataoka, K. *Bioconjugate Chem.* **1992**, *3*, 295−301.
(25) Wiedmann, T. S.; Kamel, L. *J. Pharm. Sci.* **2002**, *91*, 1743−1764.
(26) Francis, M. F.; Cristea, M.; Winnik, F. M. *Pure Appl. Chem.* **2004**, *76*, 1321−1335.
(27) Kim, S.; Shi, Y; Kim, J. Y.; Park, K.; Cheng, J.-X. *Expert Opin.* **2010**, *7*, 49−62.
(28) Lipinski, C. A. Drug-like properties and the causes of poor solubility and poor permeability. *J. Pharmacol. Toxicol. Methods* **2000**, *44*, 235−249.
(29) van Nostrum, C. F. *Adv. Drug Delivery Rev.* **2004**, *56*, 9−16.
(30) Lakowicz, J. R. *Principles of Fluorescence Spectroscopy*; Plenum, New York. 1999.
(31) Bevington, P. R.; Robinson, D. K. *Data Reduction and Error Analysis for the Physical Sciences*, 2nd ed.; WCB/McGraw-Hill: Boston, 1992.; Chapter 8.
(32) Biondic, M. C.; Erra-Balsells, R. *J. Chem. Soc., Perkin Trans.* **1997**, *2*, 1323−1328.
(33) Gonzalez, M. M.; Arnbjerg, J.; Denofrio, M. P.; Erra-Balsells, R.; Ogilby, P. R.; Cabrarizo, F. M. *J. Phys. Chem. A* **2009**, *113*, 6648−6656.
(34) Mallick, A.; Chattopadhyay, N. *Biophys. Chem.* **2004**, *109*, 261−270.
(35) Muller, N. *Reaction Kinetics in Micelles* In Cordes, E. A., Ed.; Plennum: New York, 1973.
(36) Kalyanasundram, K.; Thomas, J. K. *J. Am. Chem. Soc.* **1977**, *99*, 2039−2044.
(37) Berr, S.; Jones, R. R. M.; Johnson, J. S. *J. Phys. Chem.* **1992**, *96*, 5611−5617.
(38) Chakraborty, H.; Banerjee, R.; Sarkar, M. *Biophys. Chem.* **2003**, *104*, 315−325.
(39) Rottman, C.; Avnir, D. *J. Am. Chem. Soc.* **2001**, *123*, 5730−5734.
(40) Partearroyo, M. A.; Alonso, A.; Goni, F. M.; Tribout, M.; Paredes, S. *J. Colloid Interface Sci.* **1996**, *178*, 156−159.
(41) Weidemaier, K.; Tavernier, H. L.; Fayer, M. D. *J. Phys. Chem. B* **1997**, *101*, 9352−9361.
(42) Saroja, G.; Ramachandram, B.; Saha, S.; Samanta, A. *J. Phys. Chem. B* **1999**, *103*, 2906−2911.
(43) Shannigrahi, M.; Bagchi, S. *Chem. Phys. Lett.* **2004**, *396*, 367−371.
(44) Almgren, M.; Grieser, F.; Thomas, J. K. *J. Am. Chem. Soc.* **1979**, *101*, 279−291.
(45) (a) Arnaut, L. G.; Formosinho, S. J. *J. Photochem. Photobiol. A* **1993**, *75*, 1−20. (b) Zhao, J.; Ji, S.; Chen, Y.; Guo, H.; Yang, P. *Phys. Chem. Chem. Phys.* **2012**, *14*, 8803−8817. (c) Kosower, E. M.; Huppert, D. *Annu. Rev. Phys. Chem.* **1986**, *37*, 127−156. (d) Agmon, N. *J. Phys. Chem. A* **2005**, *109*, 13−35.
(46) Paul, B. K.; Guchhait, N. *Spectrochim. Acta A* **2011**, *81*, 590−597.
(47) Esposito, C.; Colicchio, P.; Facchiano, A.; Ragone, R. *J. Colloid Interface Sci.* **1998**, *200*, 310−312.
(48) Geng, F.; Yu, L.; Lu, T.; Li, Z.; Zheng, L.; Li, G. *J. Dispersion Sci. Technol.* **2008**, *29*, 1209−1213.
(49) Lopez, O.; Cocera, M.; Pons, R.; Azemar, N.; Lopez-Iglesias, C.; Wehrli, E.; Parra, J. L.; de la Maza, A. *Langmuir* **1999**, *15*, 4678−4681.
(50) Vazquez, M. E.; Blanco, J. B.; Imperiali, B. *J. Am. Chem. Soc.* **2005**, *127*, 1300−1306.
(51) Sytnik, A.; Kasha, M. *Proc. Natl. Acad. Sci. U.S.A.* **1994**, *91*, 8627−8630.
(52) Reichardt, C. *Chem. Rev.* **1994**, *94*, 2319−2358.
(53) Saroja, G.; Samanta, A. *Chem. Phys. Lett.* **1995**, *246*, 506−512.
(54) Dennison, S. M.; Guharay, J.; Sengupta, P. K. *Spectrochim. Acta A* **1999**, *55*, 903−909.
(55) Kalyansundram, K.; Thomas, J. K. *J. Phys. Chem.* **1977**, *81*, 2176−2180.
(56) Paul, B. K.; Guchhait, N. *J. Colloid Interface Sci.* **2011**, *363*, 529−539.
(57) Demchenko, A. P. *Luminesc.* **2002**, *17*, 19−42.
(58) Samanta, A. *J. Phys. Chem. B* **2006**, *110*, 13704−13716 and references therein..
(59) During REES measurements meticulous care has been devoted to the selection of excitation wavelength to ensure that the variation of λ_{ex} involves shifting to the red end of the absorption spectra and not merely the absorption maxima. This is a very crucial criterion for REES monitoring.[57,58]
(60) Pramanik, R.; Sarkar, S.; Ghatak, C.; Rao, V. G.; Mandal, S.; Sarkar, N. *J. Phys. Chem. B* **2011**, *115*, 6957−696.
(61) Ashby, K. D.; Das, K.; Petrich, J. W. *Anal. Chem.* **1997**, *69*, 1925−1930.
(62) Rosen, M. J. *Surfactant and Interfacial Phenomena*; Wiley Inter-Science: New York, 1978.
(63) Bhattacharyya, K. *Acc. Chem. Res.* **2003**, *36*, 95−101.
(64) Dutt, G. B. *J. Phys. Chem. B* **2003**, *107*, 10546−10551.
(65) Dutta Choudhury, S.; Mohanty, J.; Pal, H.; Bhasikuttan, A. C. *J. Am. Chem. Soc.* **2010**, *132*, 1395−1401.
(66) Quitevis, E. L.; Marcus, A. H.; Fayer, M. D. *J. Chem. Phys.* **1993**, *97*, 5792−5769.

(67) Chakraborty, A.; Seth, D.; Setua, P.; Sarkar, N. *J. Chem. Phys.* **2008**, *128*, 204510−204519.
(68) Ghatak, C.; Rao, V. G.; Pramanik, R.; Sarkar, S.; Sarkar, N. *Phys. Chem. Chem. Phys.* **2011**, *13*, 3711−3720.
(69) Paul, B. K.; Guchhait, N. *Phys. Chem. Chem. Phys.* **2012**, *14*, 8892−8902.